J Mater Sci: Mater Electron (2017) 28:8218–8230
DOI 10.1007/s10854-017-6533-2

One step synthesis of a hybrid Ag/rGO conductive ink using a complexation–covalent bonding based approach

Wendong Yang[1] · Changhai Wang[1] · Valeria Arrighi[2] · Filipe Vilela[2]

Received: 15 November 2016 / Accepted: 1 February 2017 / Published online: 3 March 2017

Abstract Hybrid inks formulated using silver nanoparticles with graphene or graphene oxide (GO) have been of significant interest in development of conductive inks for manufacturing of flexible devices and systems. So far all of the methods for synthesizing these inks are based on a two-step process using silver nanoparticles. Herein, we report an Ag/rGO hybrid ink formulated by a one step method through a complexation–covalent bonding process of silver acetate and ethanolamine together with reduced graphene oxide (rGO). Successful dispersion of rGO in the alcohol based solvent was achieved by decorating rGO platelets with ethanolamine. The synthesized ink was just composed of 13.5 wt% of silver and 0.1 wt% rGO but has a favorable electrical performance. A remarkable improvement of resistivity by a factor of above 200 has been observed in Ag/rGO films sintered at 150 °C as compared with that of the Ag films produced using the same formulation and thermal treatment process, while a factor of 10 was observed at 165 °C. The enhancement of conductivity was significant up to the sintering temperature of 230 °C beyond which the difference between the Ag/rGO and Ag films are negligible. The increase of conductivity in Ag/rGO films at low temperatures was attributed to the role of rGO platelets in forming bridges to facilitate charge transfer between the silver particles.

✉ Changhai Wang
C.Wang@hw.ac.uk

[1] Institute of Sensors, Signals and Systems, School of Engineering and Physical Sciences, Heriot-Watt University, Edinburgh EH14 4AS, UK

[2] Institute of Chemical Sciences, School of Engineering and Physical Sciences, Heriot-Watt University, Edinburgh EH14 4AS, UK

1 Introduction

Flexible electronics is a rapidly expanding research area covering the development of a wide range of electronic and energy storage devices as well as systems such as touch screens [1], sensors [2], field-effect transistors [3], photovoltaic cells [4], light-emitting diodes [5] and electrochemical energy storage systems [6]. The market for flexible electronics has been estimated to exceed $300 billion over the next 20 years [7]. Clearly, flexible electronics will play a major role in future electronic devices and systems in the coming decades.

Conductive inks have been of significant interest in the manufacture of flexible electronics for cost-effective fabrication of conductive tracks and functional devices by a variety of deposition methods such as such as inkjet, screen, flexographic, or gravure based printing methods. Numerous kinds of conductive ink with different fillers including polymers [8], carbon nanotubes [9, 10], graphene [11] and metal nanoparticles or organic metal complexes [12–40], have been developed for flexible electronics applications. Among these, silver inks have attracted significant attention due to their good electrical conductivity and strong anti-oxidant characteristics compared with copper inks. Several kinds of silver inks with nano-silver particles as fillers or organic silver fillers have been developed and used in the formation of conductive traces [12–20].

With high charge carrier mobility, superlative thermal and chemical stability and intrinsic flexibility, graphene is considered to be a very promising ink material [41]. Although high quality graphene can be fabricated by versatile synthetic routes (bottom-up or top-down process) [42–48], pristine or pure graphene still shows poor solubility in common solvents such as water, which is not

ideal for formulation of conductive inks. Graphene oxide (GO) is a favorable candidate due to its good solubility and can be easily formulated into inks. But the electric conductive of GO is poor and usually require an additional reduction process (chemical or photo or thermal) to make the ink tracks conductive, which has cost and safety implications.

Reduced graphene, or rGO is the reduction derivative of GO and has similar electrical, thermal and mechanical properties compared with the pristine graphene. In addition, rGO contains some residual defects and organic groups on its surface, which are easily functionalized for different applications. These characteristics make the rGO an ideal ink material for flexible electronics compared to pure graphene. However, the conductivity of films from rGO inks is usually low. Also, solvents used to disperse the poor hydrophilic rGO, such as N,N-dimethylformamide (DMF), N-methyl-2-pyrrolidone (NMP), dimethyl sulfoxide (DMSO), are not environmentally benign.

Recently there has been a significant interest in the development of hybrid inks from graphene or its derivatives decorated with silver nanoparticles. Li et al. prepared inks of Ag and rGO, one based on a mixture of Ag nanotriangle particles (NTPs) and rGO platelets, and the other containing polyhedral Ag and rGO nanoparticles [49]. The Ag NTP–rGO patterns displayed a low sheet resistance of 170 Ω/□ with a transmittance of 90.2%. One disadvantage of this method is its final reduction process, which is too time-consuming (3 h at 110 °C in a vacuum oven after the ink printing process). Xu et al. prepared a hybrid conductive ink composed of Ag nanoparticles (NPs) and graphene–Ag nanocomposites for writing electronics [50]. Zhang et al. synthesized a Ag/rGO composite with good conductivity and dispersibility as a conductive ink filler for inkjet printing [51]. Multifarious regular patterns with an optimum conductivity of 2.0×10^3 S/m and a sheet resistivity of 0.5 kΩ/□ were fabricated using a standard commercial inkjet printer. Although various kinds of graphene/silver hybrid inks have been created and deposited onto different substrates and conductive patterns have been obtained, they are still not economically feasible because of the low throughput, the complexity of the process as well as the utilization of toxic chemicals. To date, all of these inks are synthesized based on a two-step process where the silver/graphene or silver/rGO composites are first prepared by a complex chemical reduction process and are then formulated into inks. The process is not facile. Besides, the amount of ink produced by these methods is usually low, which limits their potential for commercial development. Moreover, the chemicals used for synthesizing such inks such as hydrazine or DMF, are not ideal because they are toxic and not environmentally friendly. Therefore, it will be advantageous to develop new hybrid inks using non-toxic solvents and a one-step synthetic method.

In this paper, we report the first development of a one-step method for the synthesis of a Ag/rGO hybrid ink composed of organic silver complex and rGO. Our approach has the following advantages. First, the ink formulation process is only one-step, facile, high throughput as well as environmentally friendly, which is different from all the current existing methods used for synthesizing silver/rGO hybrid inks and are potentially easy for industrial production. Second, the dispersion of rGO in the alcohol based solvent can be obtained. Third, the synthesized ink is composed of 13.5 wt% of silver and 0.1 wt% rGO but has a favorable electrical performance at low temperature (150 °C), which not only enhances conductivity but also reduces the cost of the organic silver complex based inks. The thermal response of the ink has been studied to understand the chemical changes in it. The formation and conductive mechanism of the rGO/Ag films from the ink were investigated, including the sintering temperature, time and the degree of interaction between the Ag particles. As shown later, our work shows that significant improvement of conductivity, by more than a factor of 200, can be obtained compared to the Ag films sintered at the same temperature of 150 °C. The resistivity of the Ag/rGO films is consistently lower than that of the Ag films at sintering temperatures up to 230 °C. A model for the mechanism of conductivity enhancement in Ag/rGO films has been proposed.

2 Experimental section

2.1 Materials

Silver acetate, ethanolamine, ethylene glycol, ethanol and oleic acid were obtained from Sigma-Aldrich and were used as received without further purification. The rGO powder was supplied by Graphenea and was produced by chemical reduction of graphene oxide. The size of the rGO platelets is in the range of 260–295 nm. The BET surface area is 422.69–499.85 m^2/g. The solubility is below 0.1 mg/ml in NMP, DMSO and DMF. The conductivity is above 600 S/m. The chemical compositions are: C (77–87%), H (0–1%), O (13–22%), and N (0–1%). The polyimide (PI) substrate was a Kapton film from DuPont (500 HN, 127 μm in thickness). For surface modification, PI films of (15×15 mm^2) were cleaned with ethanol and de-ionized water to remove particles and organic contamination prior to the surface modification process.

2.2 Synthesis

The silver/rGO ink was prepared using a modified process of the previous work [17] to study the effect of rGO on the conductivity of the resultant films and to reduce the amount of silver in the film thus reducing the ink cost in electronic applications: rGO powder (6 mg) was first dispersed in 5 ml of a mixed solvent containing ethanol (2 ml), ethylene glycol (2.85 ml) and oleic acid (0.15 ml) by sonication for 30 min, and then silver acetate (1.6 g) was added into the solution. After stirring for 10 min, ethanolamine (1.2 ml) was added. The mixture was stirred for 60 min to form the ink. It is useful to note that the appearance of the solution changed, from the initial suspension to a homogeneous solution. For comparison of the electrical performance of films with rGO, Ag films were obtained using the same ink formulation but without rGO and were produced using the same deposition and sintering processes.

2.3 Ink deposition and sintering

For surface modification, the PI films were processed in an alkaline solution containing 10% sodium hydroxide at 30 °C for 60 min. Then, the Ag/rGO ink was deposited on the modified PI films by a drop-coating method, and sintered at selected temperatures for up to 60 min. The film thickness was controlled by the volume of ink solution deposited onto the PI film.

2.4 Characterization

UV–Vis spectra were obtained on an EV300 UV–Vis spectrophotometer. Fourier transform infrared spectra in the range of 400–4000 cm^{-1} were recorded on a Perkin Elmer Spectrum 100 FT-IR spectrometer. The thermal profile was measured under nitrogen atmosphere by differential scanning calorimetry (DSC, Thermal Advantage DSC 2010) at a heating rate of 10 °C min^{-1} from room temperature to 300 °C. The crystalline structure of the Ag/rGO films was measured by X-ray diffraction (XRD) using Cu Kα and λ = 0.15418 nm. The surface morphology of the Ag/rGO films was obtained on a Leo 1530 VP Field Emission scanning electron microscope (SEM). The chemical composition was determined on an Oxford X-maxN 150 surface energy disperse spectrometer (EDS). The sheet electrical resistivity was measured using a multi-height probe station (Jandel Engineering, UK) with tungsten probe tips of 1 mm of spacing and 60 g of maximum force. The thickness of the sintered films was measured using a Zygo View 5200 white light phase shifting interferometer and was used to calculate the equivalent bulk resistivity.

3 Results and discussion

3.1 Ink chemistry

The ink was formulated through a complexation–covalent bonding process of silver acetate and ethanolamine together with the nano rGO. Silver acetate was chosen as the silver precursor since this compound has poor solubility in the solvent medium (alcohol in this case) and so the reaction rate can be controlled. Ethanolamine was used to increase the silver content of the ink to improve film deposition efficiency, decrease the sintering temperature [39] as well as to improve the dispersibility of rGO in the solvent. rGO was used to study its effect on the conductivity of the resultant Ag/rGO films and to reduce the amount of silver in the film thus reducing the ink cost in electronic applications. Ethanol was used to adjust the surface tension of the ink and ethylene glycol was chosen as a low reduction agent and a co-solvent with a high boiling point to suppress the undesirable coffee ring effect in film deposition.

The chemical reaction mechanism leading to formation of the Ag/rGO ink is described below. The lone pair of electrons on the nitrogen of ethanolamine can coordinate with silver acetate to form a silver organic complex, at room temperature, which has good solubility in alcohols due to the presence of OH groups (Eq. 1) [17]. At the same time ethanolamine can react with the rGO to yield rGO decorated with amino group; the latter has better dispersibility in alcohols due to the effects of electrostatic repulsion and volume exclusion between the decorated rGO sheets (Eq. 2).

$$CH_3COOAg + 2NH_2CH_2CH_2OH \rightarrow CH_3COOAg\left(NH_2CH_2CH_2OH\right)_2 \quad (1)$$

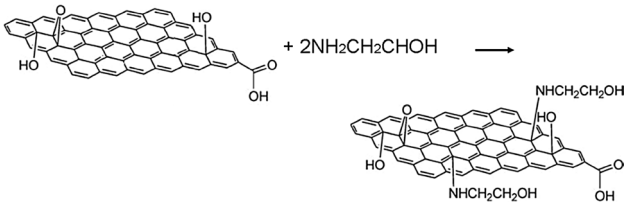

(2)

In order to verify the interaction between rGO and ethanolamine, UV–Vis spectra and FT-IR spectra were obtained for dispersions of rGO and rGO/ethanolamine in ethanol. As showed in Fig. 1, the rGO dispersion shows a typical absorption peak at 264 nm, as reported in previous work [52]. This absorption peak is attributed to the n-π* transition of C–O bonds on the surface of rGO. However, in the presence of ethanolamine, the absorption is slightly red-shifted from 264 to 270 nm, indicating that some new groups were introduced on the rGO surface and possibly

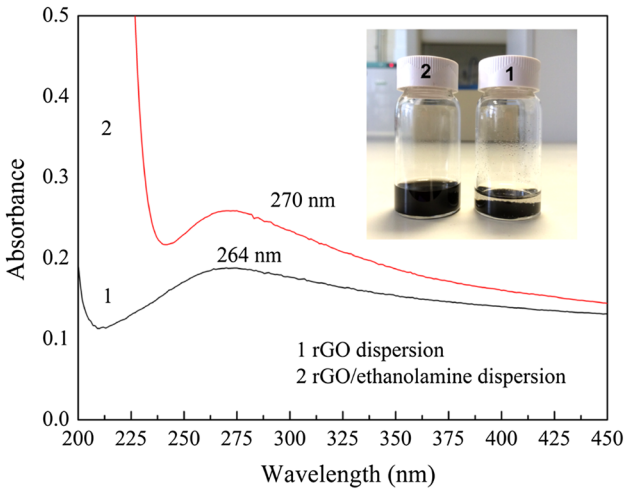

Fig. 1 UV–Vis absorption spectra of rGO and rGO/ethanolamine dispersions (*inset* is the optical image of these two kinds of dispersion)

due to the interaction with ethanolamine. The inset figure is the optical microscopy image of these two kinds of dispersion after 10 min' standing. Obviously, the stability of rGO/ethanolamine dispersion is better than that of pure rGO dispersion where rGO has gathered at the bottom of the glass bottle.

Figure 2 shows the IR spectra of rGO powder dried from the dispersions of rGO and rGO/ethanolamine in ethanol. It can be seen that several new peaks are visible in the sample with ethanolamine. The broad bands between 3100 and 3700 cm^{-1} are attributed to the vibrations of O–H and N–H. Two peaks at 2933 and 2870 cm^{-1} were attributed to the asymmetric and the symmetric CH_2 stretch, respectively. The broadening of the band at 1645 cm^{-1} can be assigned to –CONH– vibrations, indicating formation of a covalent bond of ethanolamine with rGO surface. The peak at 1430 and 1350 cm^{-1} indicates in-plane bending vibrations of the methyl group. The C–O stretching vibration is at 1055 cm^{-1}. All of the differences show that the ammonium groups from ethanolamine can react with the rGO surface, thereby resulting in its good dispersibility in a hydrophilic solvent. It has been shown in the previous study of functionalization of graphene with ethanolamine that the latter can react with the hexatomic rings of graphene oxide through covalent bonding, in our case it should be with the hexatomic rings of rGO [53].

In order to determine the reaction temperature of the ink, UV–Vis spectra were obtained after the ink was heated up to different temperatures. Once the ink was heated, a complex chemical reaction occurred between the various components, from graphene/silver complex to graphene/silver composites, which will also be explained in the subsequent text. Figure 3 shows the results of UV–Vis. measurements. At temperatures below 120 °C, there is only one absorption peak associated with the silver carboxylate-amine complex, which is at 217 nm. However after the ink was heated to 120 °C the absorption spectrum is very different, the peak at 217 nm disappears and a weak peak at 303 nm is observed. This peak is associated with silver nanostructures but different from conventional silver nanoparticles [54]. Based on these results and the previous work [17], it can be deduced that the ink underwent simultaneous change of solvent components and reduction of silver ion complex at elevated temperatures and in the process ethylene glycol changes to acetaldehyde and triggers the reduction of the silver complex. This is the start of the conversion process from the deposited ink film to the formation of conductive Ag/rGO film after thermal sintering (Fig. 4).

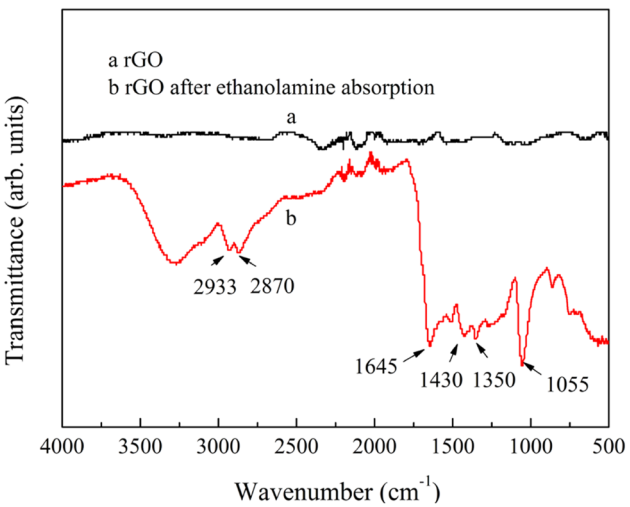

Fig. 2 FT-IR spectra of rGO and rGO after ethanolamine adsorption

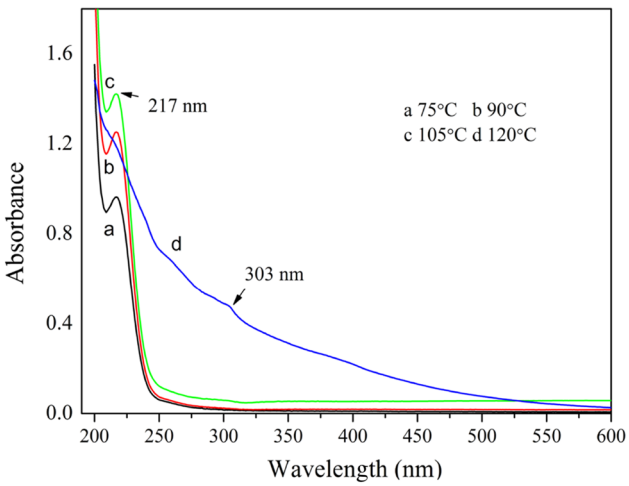

Fig. 3 UV–Vis absorption spectra of Ag/rGO ink at different heating temperatures

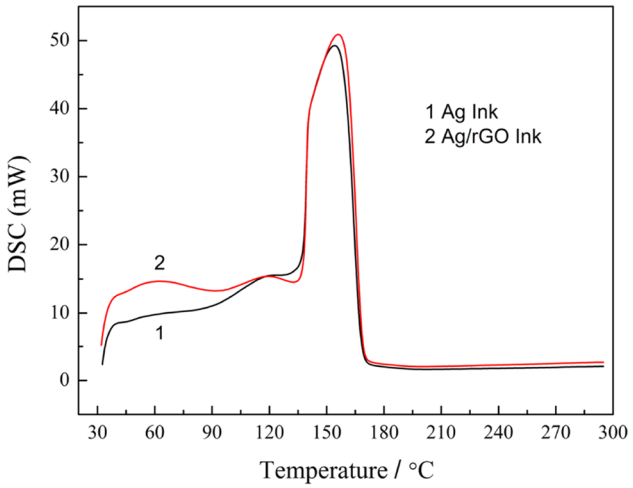

Fig. 4 DSC analysis of Ag ink and Ag/rGO ink

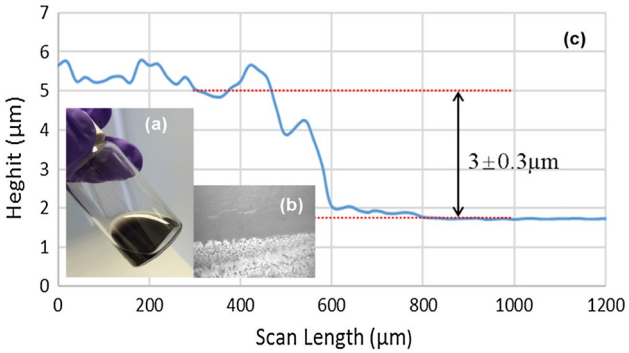

Fig. 5 **a** As-prepared Ag/rGO ink, **b, c** Optical microscopy image and surface profile of the sintered Ag/rGO film

3.2 Thermal behavior of the Ag/rGO inks

DSC analysis was carried out to investigate the thermal decomposition behavior of the as-prepared Ag and Ag/rGO inks as shown in Fig. 4 (as the amount of rGO in the ink is very low, we did not test its thermal decomposition behavior). The two endothermic peaks, at 60 and 120 °C, are related to the evaporation and decomposition of the solvents. The third endothermic peak at about 165 °C is attributed to the formation of elemental silver [27], which is much lower than the decomposition temperature of the silver acetate powder. This is because the lone pair electrons of the nitrogen atoms of ethanolamine can effectively combine with the silver to form a silver-amine complex with a lower redox potential which determines the decomposition temperature. This is similar to the thermal behavior of other silver salt based inks [27] and it is also consistent with our previous analysis of the results in Fig. 3.

3.3 Microstructure of the Ag/rGO films

Ag/rGO films were produced by drop-coating of the ink on the modified PI substrates. The sintering process was carried out on a hotplate in a chamber. Based on the DSC results and UV–Vis analysis of the ink, we used temperatures between 135 and 245 °C for thermal sintering. Figure 5 shows the as-prepared Ag/rGO ink, the corresponding optical microscopy image and surface profile of the sintered Ag/rGO film. It can be seen that the sintered film with an average thickness of 3 ± 0.3 μm has relatively uniform surface structure, with silver nanoparticles accumulated at the centre.

Figure 6 presents the XRD results of the Ag/rGO films sintered at different temperatures for 60 min (measured in 2θ from 25° to 85°). The peaks of Ag at 2θ equal to 38.2°, 44.4°, 64.5°, 77.5° and 81.6° were observed in all of the films which indicate that the silver ions are transformed to silver crystals. The reflection peaks are indexed as the (111), (200), (220), (311) and (222) crystal planes of the silver face-centered cubic (fcc) crystal structure. The XRD characteristic of the rGO powder is also shown in Fig. 6 (the bottom) which is a broad diffraction peak around 24°. However, this peak is not present in the characteristics of the Ag/rGO films which may be the results of the low content and diffraction intensity of rGO in the film. The peak intensities of the silver increased with the sintering temperature. This is because the increase in crystallization of the silver NPs in the film as the sintering was increased.

The particle sizes of the silver nanocrystals in the films formed at 135, 165, 215 and 230 °C were calculated using the Debye-Scherrer equation [39],

$$d = 0.89\lambda/\beta\cos\theta \tag{3}$$

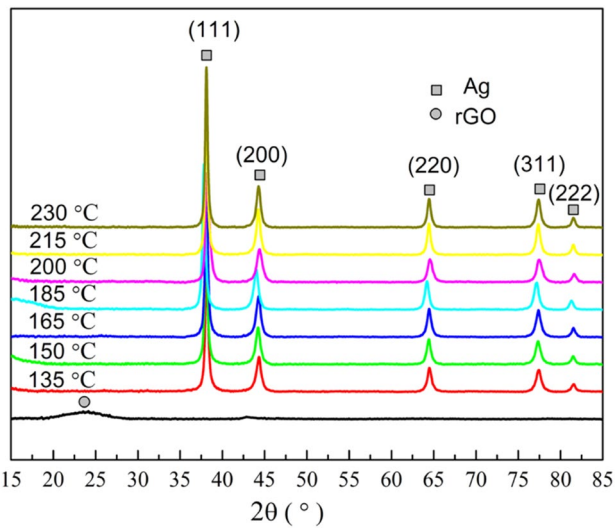

Fig. 6 XRD patterns of the Ag/rGO films sintered at different temperatures for 60 min. Data shifted vertically, for clarity

where d is the particle size, λ is the X-ray wavelength (0.15418 nm), θ is the Bragg angle and β corresponds to the full width at half-maximum (FWHM). The results are given in Table 1.

Table 1 Particle sizes of silver nanocrystals in the film at different sintering temperature

Sintering temperature (°C)	2θ (Degrees)	FWHM (â)	Size (nm)
135	38.155	0.396	21.01
165	38.118	0.377	22.06
215	38.099	0.362	22.97
230	38.109	0.358	23.24

It can be seen that the average particle size of silver nanocrystals in the film increases with the sintering temperature but the change is not significant.

The SEM images of the Ag/rGO films sintered at different temperatures are shown in Fig. 7. It can be seen that the morphology of the Ag/rGO films gradually changes with the sintering temperature and presented different microstructural changes. At lower sintering temperatures (150 °C, 165 °C), less silver nanoparticles were produced. These are relatively small (Fig. 7a, b) and surrounded by organic molecules (e.g. ethylene glycol, T_b=197 °C). The magnified images of Fig. 7b, indicate that the average size of silver nanoparticles produced is about 23 nm, which is consistent with values calculated from the XRD data. At higher sintering temperatures (185 °C, 200 °C), more silver NPs were produced. The film seems to be made up of many layers

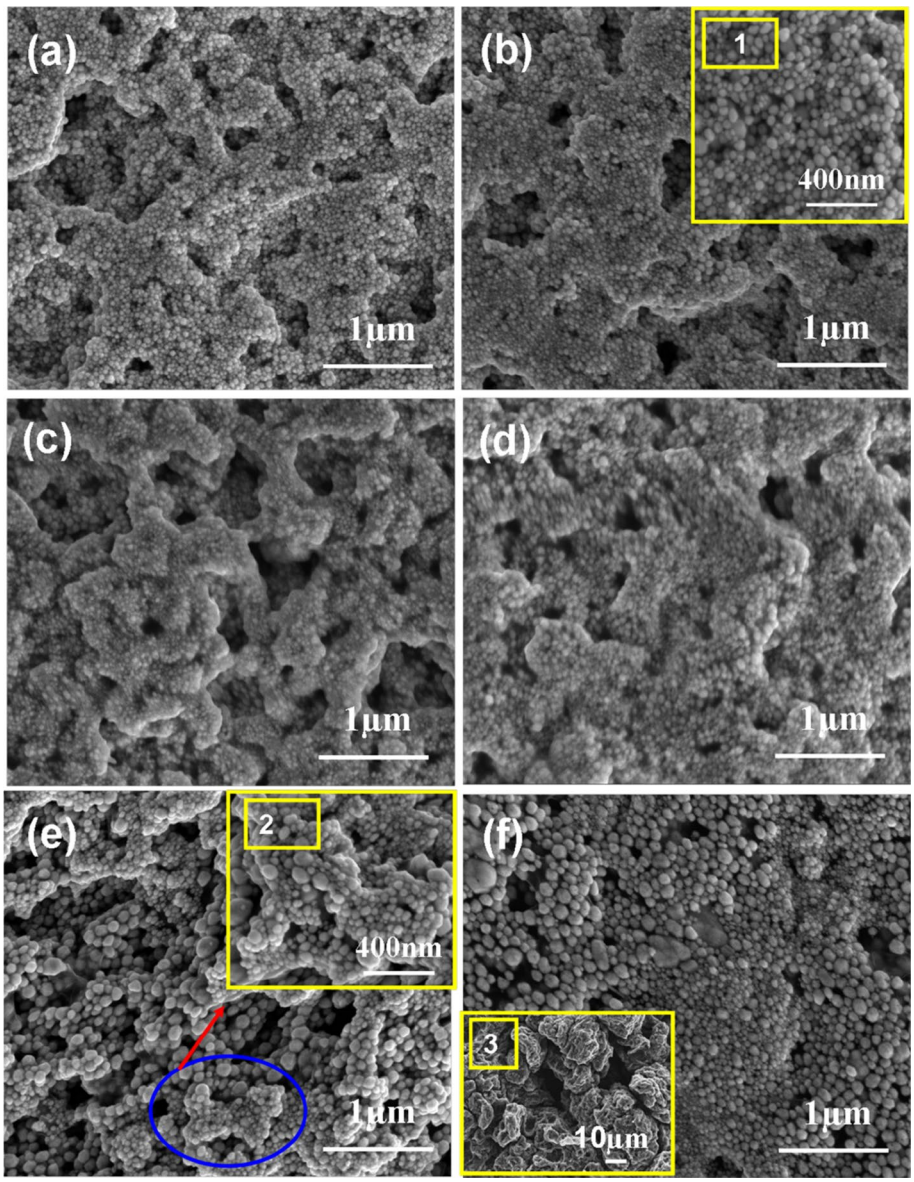

Fig. 7 SEM images of Ag/rGO films sintered at 150, 165, 185, 200, 215 and 230 °C for 60 min. (*inset* 1 and 2 are the corresponding magnified images of **b** and **e***3* corresponds to the image of rGO offered by Graphenea Website)

where silver NPs were supported (Fig. 7c). By combining information from the rGO images offered by Graphenea (Fig. 7f3), it can be deduced that these supporting layers are the graphene particles. In addition, it should be noted that pores and voids among the NPs became less and smaller at this stage, stacking density was also improved (Fig. 7d). Sintering at higher temperatures (215 °C, 230 °C) made the silver nanoparticles grow forming larger particles through neck connection (Fig. 7e2) and this further improves the stacking density of the film. By comparing Fig. 7 b1, e2, f3, it can be deduced that in the sintering process, silver ions were reduced into silver NPs and rGO serves as medium to support and bridge them.

Figure 8 shows the results of C/O ratio and Ag content from EDS based analysis. As shown in Fig. 8, the C/O ratio increases rapidly as sintering temperature was increased from 150 to 200 °C, indicating that the decomposition and volatilization of organic molecules mainly occurred at this stage. The Ag content increased from 82.76 to 86.17 wt% between 215 and 240 °C, this indicates that most of the organic molecules were decomposed and volatilized and the Ag^+ ions were reduced to Ag^0.

Considering the boiling point of the ink solvents and the heat-resisting temperature of PI substrates, we selected 230 °C as the sintering temperature to study the effect of sintering time on the microstructure of the silver films. The samples were obtained by sintering the ink films on modified PI substrates for 5, 15, 30, 45 and 60 min and were evaluated by SEM and XRD methods.

As shown in Fig. 9, silver ions could be transformed to silver crystals within 5 min. With the increasing sintering time, the peak intensity also increases, indicating that more metallic silver was formed. The particle sizes of silver nanocrystals in the films were calculated using Eq. (1) and

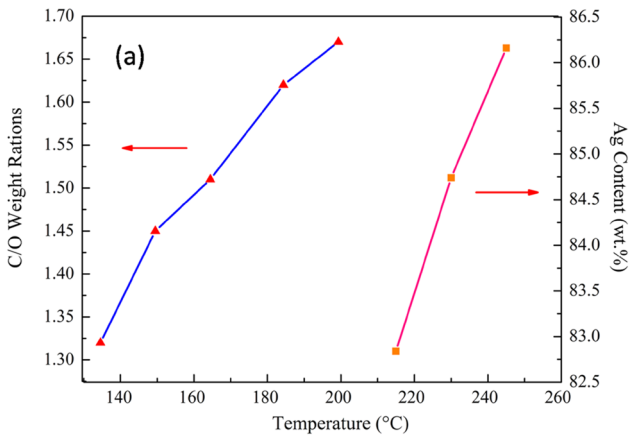

Fig. 8 Change of C/O weight ratio and Ag content in Ag/rGO films as a function of sintering temperature

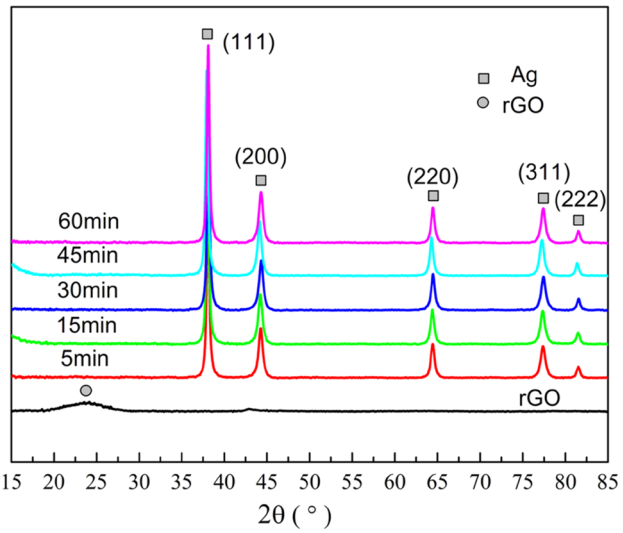

Fig. 9 XRD patterns of Ag/rGO films prepared with the inks after sintering at 230 °C for 5, 15, 30, 45 and 60 min

the results are shown in Table 2. As shown in Table 2, the increase in particle size is very small.

The SEM images in Fig. 10 show the microstructures of Ag/rGO films produced using different sintering times. Significant differences in the morphologies of Ag/rGO films can be observed. When the sintering time was 5 min, silver nanoparticles were produced but still surrounded by organic molecules (Fig. 10b). Besides, there are many holes in the film and it is not uniform (Fig. 10a). When the sintering time was increased, more silver particles were generated (Fig. 10c). More particles were in contact and the stacking density was improved due to the evaporation of the solvents and decomposition of the organic silver complexes (Fig. 10d). When the sintering time was further increased to 60 min, even more silver nanoparticles were produced and formed a dense structure (Fig. 10e, f).

The chemical compositions of the Ag/rGO films sintered at 230 °C for 5, 15, 30, 45 and 60 min were studied by EDS. The results are shown in Fig. 11. Clearly, three elements (C, O, and Ag) were found to exist in the films which originated from the chemical elements in the ink. As the sintering time was increased from 5 to 60 min, the Ag content increased from 80.16 to 86.17 wt%, the content of C decreased from 11.44 to 7.98 wt% while the oxygen decreased from 8.4 to 5.85 wt%. The results indicate that more metallic silver nanoparticles were formed and organic molecules were decomposed and volatilized. The small amount of organic residue may be from the OA (T_b=360 °C).

Based on the composition of the ink, the percentage of C_{OA} in the ink can be calculated as 1.31%. Using the above EDS result of 7.98% for carbon in the films obtained at

Table 2 Particle sizes of silver nanocrystals in the film sintered at 230 °C for different times

Sintering time (min)	2θ (Degrees)	FWHM (β)	Size (nm)
5	38.035	0.368	22.59
15	38.040	0.365	22.80
30	38.056	0.360	23.11
60	38.109	0.358	23.24

230 °C for 60 min sintering, the amount of C from the other chemicals in the solvents and rGO in the sintered film is estimated to be 6.67%. Since the amount of rGO in the ink is very small, so the carbon in the sintered film is mostly from the organic residues associated with the solvents. This is similar to the results reported previously for the sintered silver films from an organic silver ink which showed carbon content of 4.29 wt% in the sintered silver films [18]. This may also be one of the reasons why the electrical properties of the ink based silver films are not as good as that of the bulk silver.

Based on the DSC, UV–Vis, SEM and EDS results, it can be deduced that, during sintering process, the films

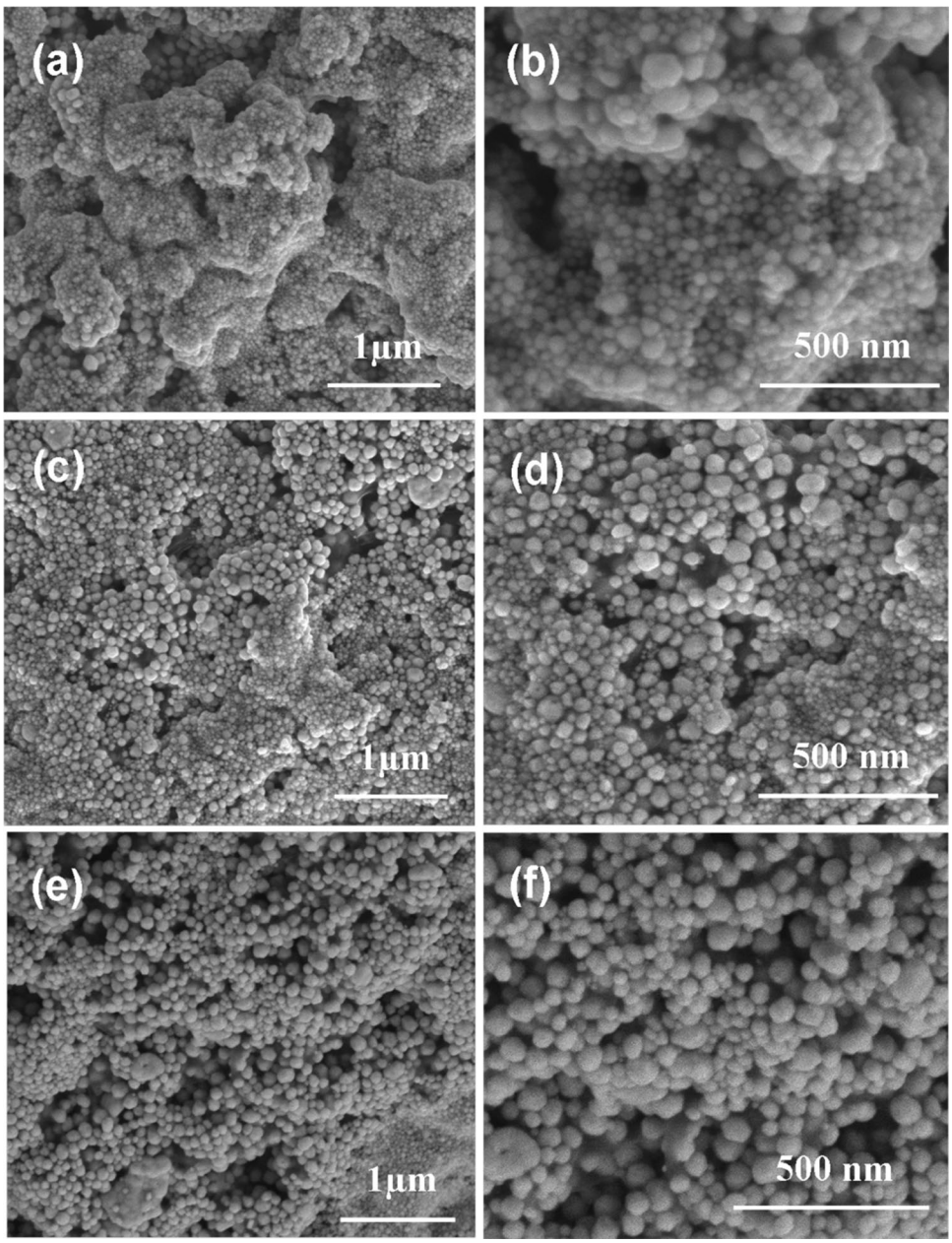

Fig. 10 SEM images of Ag/rGO films sintered at 230 °C for 5, 15 and 60 min (**a, c, e**) and corresponding magnified images (**b, d, f**)

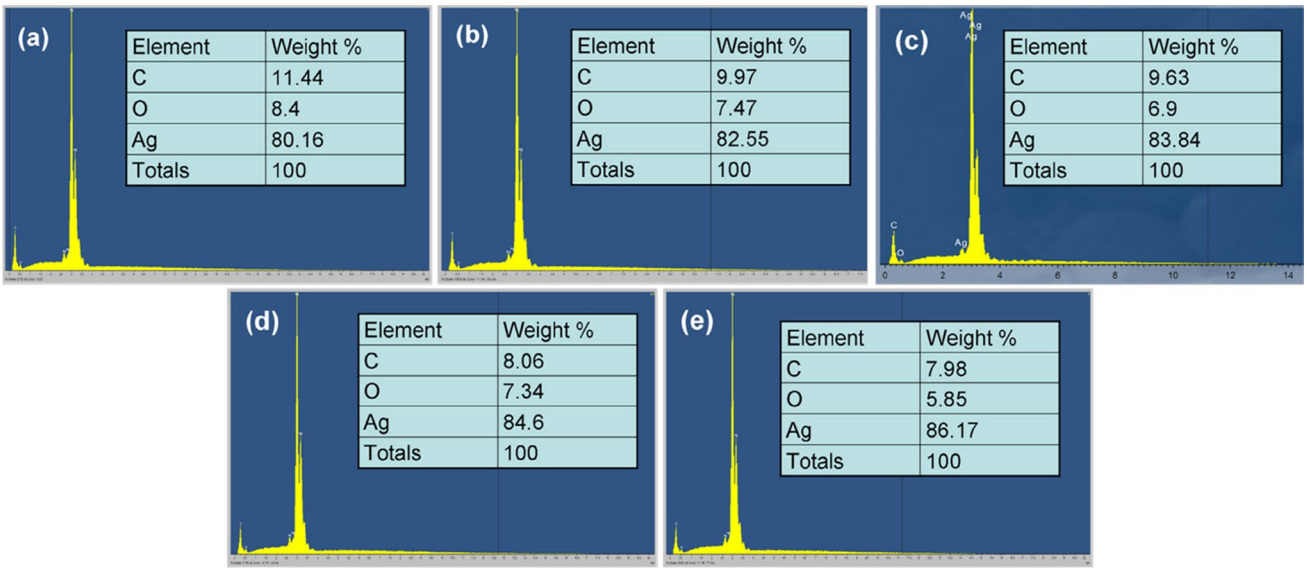

Fig. 11 EDS results of Ag/rGO films formed at 230 °C for **a** 5, **b** 15, **c** 30, **d** 45 and **e** 60 min

underwent a series of processes including solvent evaporation, reduction of silver ions and neck connection of the silver nanoparticles during the sintering process.

3.4 Electrical and flexible performance

For comparison of the electrical performance of films with rGO, Ag films were obtained using the same ink formulation but without rGO. The Ag films were produced using the same deposition and sintering processes for the Ag/rGO films. The resistivities of the Ag and Ag/rGO ink films were calculated from the measured sheet resistance and film thickness using the following equation,

$$\rho = R_s \times t \tag{4}$$

where ρ is the resistivity, R_s is the sheet resistance of the Ag or Ag/rGO film, t is the average thickness of the Ag and Ag/rGO film which was measured to be about 3 ± 0.3 μm. To be precise, the sheet resistance of each sample was test at least three times and took the average.

Calculated resistivity values for the Ag and Ag/rGO films are plotted in Fig. 12 as a function of sintering temperature. In both cases the resistivity decreases rapidly by several orders of magnitude as the sintering temperature was increased from 150 to 245 °C. The resistivity of the Ag films decreased from 188.75 to 1.78×10^{-5} Ω cm, while the resistivity of Ag/rGO film decreased from 0.728 to 1.47×10^{-5} Ω cm. Below 150 °C, the resistivity is very high and is beyond the sensitivity of the 4-probe instrument. The Ag/rGO film has much lower resistivity than the Ag film when the sintering temperature is below 230 °C with the maximum enhancement by a factor of 200 achieved at

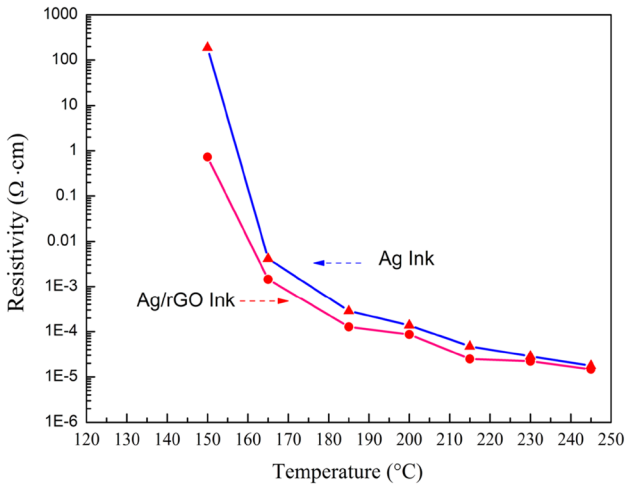

Fig. 12 Resistivity variation of the deposited Ag and Ag/rGO films sintered at various temperatures for 60 min

150 °C. It is worth noting that the resistivity of the Ag/rGO film sintered at T < 165 °C was below 10^{-4} Ω cm, which is sufficient for some applications; the sintering temperature is comparable with heat-sensitive flexible substrates such as PET. The enhancement in film conductivity will be discussed in Sect. 3.5.

Figure 13 shows the effect of sintering time on the resistivity of the films at the sintering temperature of 230 °C. The resistivity decreased by a factor of about 5 for both of the Ag and Ag/rGO films when the sintering time was increased from 5 to 60 min. However, the reduction of resistivity in the Ag/rGO film is much faster than in the Ag film, reaching the same value in 30 min as compared

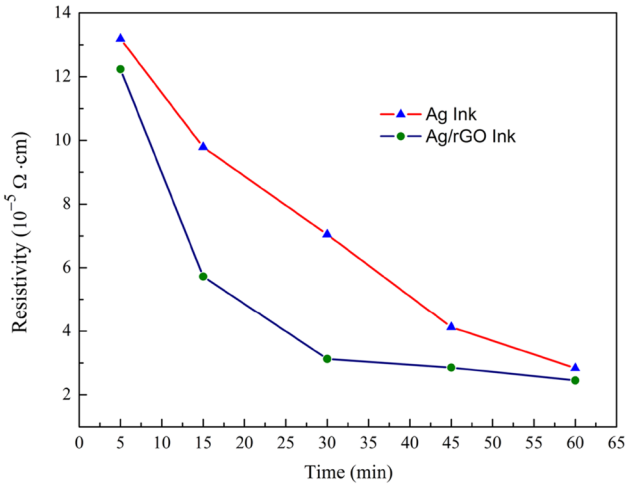

Fig. 13 Resistivity of the deposited Ag/rGO films as a function of sintering time at 230 °C

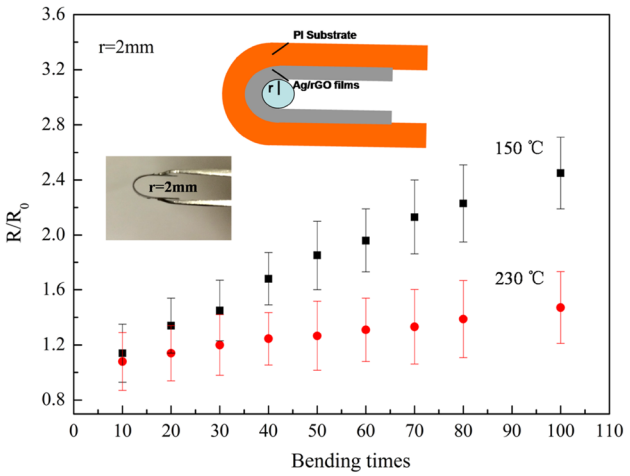

Fig. 14 Flexibility test of Ag/rGO obtained at 150 and 230 °C on PI substrate (*Inset* is the schematic diagram of bending test)

to 60 min in the case of the Ag film. Therefore the results highlight another advantage of using the Ag/rGO hybrid ink for formation of conductive tracks for electronic and energy storage devices and sensors.

Apart from the electrical performance, flexibility is another import characteristic ink based conductor tracks, which is assessed for our samples as showed in Fig. 14. The cyclical bending tests were conducted on the Ag/rGO film obtained at 150 and 230 °C (1.5 cm × 7.5 mm) on PI substrates. The test was carried out by compressing the sample for a given radius of curvature (r = 2 mm) [55]. R_0 and R denote the sheet resistance of the Ag/rGO film before and after the bending tests. It can be seen that resistance of the film obtained at 230 °C shows a small increase after 100 times of bending, implying the films have good flexibility. The resistance of the film obtained at 150 °C doubles after the same number of bending. The increase in resistance may be the result of reduced contact between silver nanoparticles in the film (Fig. 15b).

3.5 Conduction mechanism

It is well known that the conduction mechanisms in conductive inks are mainly explained in terms of two theories: the percolation threshold theory [56] and the tunneling effect or field emission [57]. In the percolation theory, there is a dramatic decrease in resistivity when the particles' content in the ink film reaches a critical value. In the tunneling effect, electrons in one particle can penetrate the potential barrier and reach the next particle within a critical separation distance. Conductive channels are formed before direct contact between particles. The conduction mechanism of the silver/rGO ink should be a combination of these two processes.

Figure 15 shows an illustration of intermediate processes occurring in the transformation of the Ag/RGO ink into a conductive film during the sintering process.

At a lower sintering temperature (<150 °C), less silver particles are produced by the reduction of ethylene glycol. These are likely to be surrounded by organic molecules such as ethanolamine (T_b=170 °C) and oleic acid (T_b=360 °C) and, as indicated by SEM images, have limited contact area (Fig. 15b) since the temperature is below the boiling point of these solvents. Therefore the NPs cannot form a continuous conductive network and the resistivity is very high.

When the temperature is above 150 °C, more organic molecules were decomposed and vaporized and more silver particles are generated. The silver particles form clusters resulting in an improved contact and film density. Moreover, the thickness of the surrounding organic layer separating the silver particles is decreased, which enables the quantum tunneling effect to occur and electrons can cross the barrier between the adjacent silver particles through thermal vibration to form electron paths [58], so the resistivity decreases greatly (Fig. 15c). In this process, rGO platelets play an important role in serving as a bridge for charger transfer between silver nanoparticles, thus improving the conductivity of the film due to its high carrier mobility and excellent thermal conductivity (Fig. 15d). Therefore, the resistivity of Ag/rGO film decreases more drastically than that of Ag films at the same sintering temperature.

Finally when the sintering temperature is above 200 °C, the resistivity decreases slowly, this indicates that the percolation threshold is reached. In this case almost no solvent is left in the film and all Ag^+ ions have been reduced to Ag^0. The silver particles form a continuous conductive

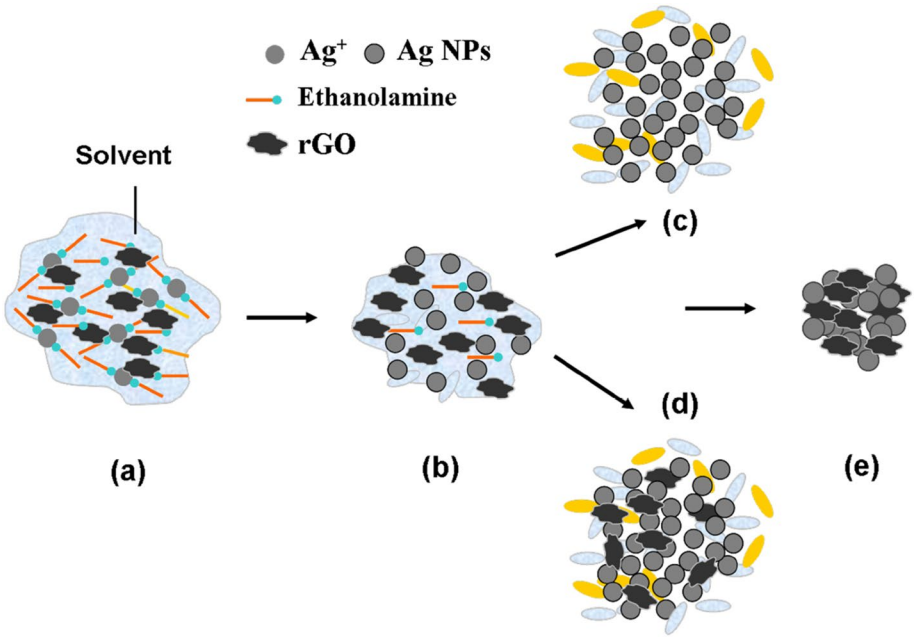

Fig. 15 Schematic illustration for the conductive mechanism of the Ag/rGO

track and cover the rGO (Fig. 15e). So the resistivity of both films is similar and the effect of rGO is less significant at higher sintering temperatures.

Within a certain range of temperature (200–500 K), an activated behavior of the Arrhenius type is commonly observed,

$$\sigma(\mathrm{T}) = \sigma_0 \exp[-E_a/(k_0 T)] \quad (5)$$

where σ is the conductivity (S/cm) at temperature T (Kelvin); σ_0 represents the nominal conductivity at infinite temperature; E_a is activation energy for the conduction process; k_0 is Boltzmann's constant (1.38×10^{-23} J/K). From Eq. (1), we can obtain:

$$\ln\sigma = \ln\sigma_0 - E_a/(k_0 T) \quad (6)$$

By plotting ln σ as a function of 1/T, the slope of the line ($-E_a/k_0$) can be obtained and thus the activation energy of the conduction process in the material can be calculated. As shown in Fig. 16, lnσ (from Fig. 12) follows an approximately linear trend as 1/T. Using the slope of the line for each film, the activation energies were determined to be 2.63×10^{-22} and 1.73×10^{-22} J for the Ag and Ag/rGO ink respectively. The results show that addition of rGO reduces the activation energy of the Ag ink significantly, thus reducing the thermal energy required to obtain good film conductivity in the sintering process.

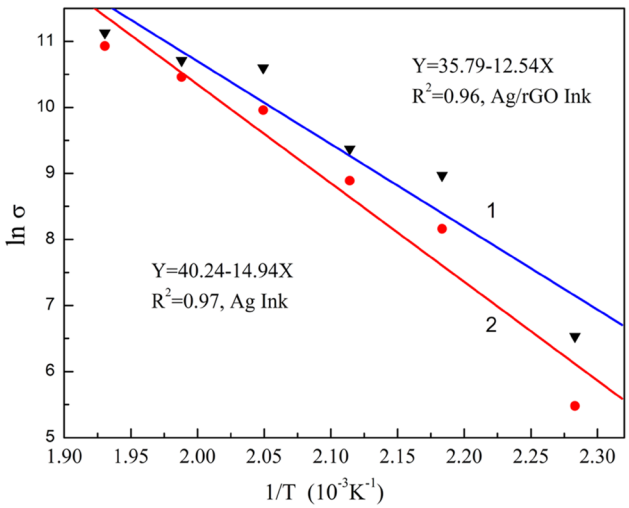

Fig. 16 Arrhenius plot of electrical conductivity

4 Conclusions

A one-step method for the synthesis of a Ag/rGO hybrid ink has been developed based on the amino complexation and the covalent bonding process of silver ions and rGO. Successful dispersion of rGO in the alcohol based solvent was achieved by decorating rGO platelets with amino groups. The thermal response of the inks and the chemical reactions were studied by DSC and spectroscopic measurements. The results show that the ink underwent simultaneous evaporation and decomposition of solvents as well as reduction of the silver ion complex. Solid Ag/rGO films have been obtained using a drop-coating method and the subsequent thermal sintering. The effects of temperature and time of thermal treatment on film composition, microstructure and electrical resistivity have been investigated. The Ag/rGO films have much better electrical

properties than the Ag films at lower sintering temperatures (150–200 °C) and there is negligible difference above 200 °C. A remarkable improvement in resistivity by a factor of above 200 has been observed in Ag/rGO films as compared to that of the Ag films after thermal treatment/sintering at 150 °C, while a factor of 10 was obtained at 165 °C. The resistivity improvement of the Ag/rGO films is attributed to the rGO platelets which facilitate electron transfer between the silver particles. The activation energies in the conduction process in Ag and Ag/rGO films have been determined and the values are 2.26×10^{-22} J and 1.73×10^{-22} J respectively.

Although progress has been made to develop a Ag/rGO hybrid ink through a simple method and significant improvement of conductivity has been observed at low temperature (150 °C), the obtained film conductivity at this temperature is still low for some applications. Therefore further research will be carried out in this area.

Acknowledgements The authors are grateful to Dr David Watson and Dr Jim Buckman for their assistance in the surface profilometry and EDX work respectively. Graphenea is thanked for supplying rGO. Wendong Yang is supported by an EPSRC DTP studentship.

References

1. J. Lee, P. Lee, H.B. Lee, S. Hong, I. Lee, J. Yeo, S.S. Lee, T.-S. Kim, D. Lee, S.H. Ko, Adv. Funct. Mater. **23**, 4171 (2013)
2. C.T. Wang, K.Y. Huang, D.T.W. Lin, Y.C. Hu, Sensors **10**, 5054 (2010)
3. H. Okimoto, T. Takenobu, K. Yanagi, Y. Miyata, H. Shimotani, H. Kataura, Y. Iwasa, Adv. Mater. **22**, 3981 (2010)
4. J.Y. Kwon, D.H. Lee, M. Chitambar, S. Maldonado, A. Tuteja, A. Boukai, Nano Lett. **12**, 5143 (2012)
5. J. Liang, L. Li, K. Tong, Z. Ren, W. Hu, X. Niu, Y. Chen, Q. Pei, ACS Nano **8**, 1590 (2014)
6. H. Gwon, H.S. Kim, K.U. Lee, D.H. Seo, Y.C. Park, Y.S. Lee, B.T. Ahn, K. Kang, Energy Environ. Sci. **4**, 1277 (2011)
7. A. Kamyshny, S. Magdassi, Small **10**, 3515 (2014)
8. N. Perinka, C. H. Kim, M. Kaplanova, Y. Bonnassieux, Phys. Procedia **44**, 120 (2013)
9. W.R. Small, M. in het Panhuis, Small **3**, 1500 (2007)
10. J.W. Han, B. Kim, J. Li, M. Meyyappan, Mater. Res. Bull. **50**, 249 (2014)
11. J.T. Li, F. Ye, S. Vaziri, M. Muhammed, M.C. Lemme, M. Ostling, Adv. Mater. **25**, 3985 (2013)
12. C.N. Chen, C.P. Chen, T.Y. Dong, T.C. Chang, M.C. Chen, H.T. Chen, I.G. Chen, Acta Mater. **60**, 5914 (2012)
13. S. Magdassi, M. Grouchko, O. Berezin, A. Kamyshny, ACS Nano **4**, 1943 (2010)
14. S.B. Walker, J.A. Lewis, J. Am. Chem. Soc. **134**, 1419 (2012)
15. R. Shankar, L. Groven, A. Amert, K.W. Whites, J.J. Kellar, J. Mater. Chem **21**, 10871 (2011)
16. B.Y. Ahn, D.J. Lorang, J.A. Lewis, Nanoscale **3**, 2700 (2011)
17. W.D. Yang, C.Y. Liu, Z.Y. Zhang, Y. Liu, S.D. Nie, J. Mater. Chem **22**, 23012 (2012)
18. Y. Chang, D.Y. Wang, Y.L. Tai, Z.G. Yang, J. Mater. Chem **22**, 25296 (2012)
19. C.N. Chen, T.Y. Dong, T.C. Chang, M.C. Chen, H.L. Tsai, S.W. Hwang. J. Mater. Chem **33**, 5161 (2013)
20. I. Jung, Y.H. Jo, I. Kim, H.M. Lee, J. Electron. Mater. **41**, 115 (2012)
21. W.D. Yang, C.Y. Liu, Z.Y. Zhang, Y. Liu, S.D. Nie, RSC Adv. **4**, 60144 (2014)
22. S. Jeong, S.H. Lee, Y. Jo, S.S. Lee, Y.H. Seo, B.W. Ahn, G. Kim, G.E. Jang, J.U. Park, B.H. Ryu, Y. Choi, J. Mater. Chem. C **1**, 2704 (2013)
23. Y. Dong, X.D. Li, S.H. Liu, Q. Zhu, J.G. Li, X.D. Sun, Thin Solid Films **589**, 381 (2015)
24. Q.J. Huang, W.F. Shen, Q.S. Xu, R.Q. Tan, W.J. Song, Mater. Chem. Phys. **147**, 550 (2014)
25. J.T. Wu, S.L.C. Hsu, M.H. Tsai, Y.F. Liu, S.W. Hwang. J. Mater. Chem. **22**, 15599 (2012)
26. D.Y. Wang, Y. Chang, Q.S. Lu, Z.G. Yang, Mater. Tech. **30**, 54 (2015)
27. X.L. Nie, H. Wang H, J. Zou, Appl. Surf. Sci **261**, 554 (2012)
28. D.Y. Wang, Y. Chang, Y.X. Wang, Q. Zhang, Z.G. Yang, Mater. Tech. **31**, 32 (2016)
29. Y.H. Choi, J. Lee, S.J. Kim, H.D. Yeon, Y. Byun. J. Mater. Chem. **22**, 3624 (2012)
30. Y.I. lee, Y.H. Choa, J. Mater. Chem. **22**, 12517 (2012)
31. T. Yonezawa, H. Tsukamoto, Y.Q. Yong, M.T. Nguyen, M. Matsubara, J. Mater. Chem. **6**, 12048 (2016)
32. T.Y. Dong, H.H. Wu, C. Huang, J.M. Song, I.G. Chen, T.H. Kao, Appl. Surf. Sci. **255**, 3891 (2009)
33. D.Y. Deng, Y.R. Cheng, Y.X. Jin, T.K. Qi, F. Xiao, J. Mater. Chem. **22**, 23989 (2012)
34. D.Y. Deng, Y.R. Cheng, Y.X. Jin, T.K. Qi, F. Xiao, ACS Appl. Mater. Interfaces **5**, 3839 (2013)
35. Y. Hokita, M. Kanzaki, T. Sugiyama, R. Arakawa, H. Kawasaki, ACS Appl. Mater. Interfaces **7**, 19382 (2015)
36. D.H. Shin, S. Woo, H. Yem, M. Cha, S. Cho, M. Kang, S. Jeong, Y. Kim, K. Kang, Y. Piao, ACS Appl Mater Interfaces **6**, 3312 (2014)
37. B.Y. Wang, T.H. Yoo, Y.W. Song, D.S. Lim, Y.J. Oh, ACS Appl. Mater. Interfaces **5**, 4113 (2013)
38. Y. Farraj, M. Grouchko, S. Magdassi. Chem. Commun. **51**, 1587 (2015)
39. Y. Tao, B. Wang, L. Wang, Y. Tai, Nanoscale Res. Lett. **8**, 1 (2013)
40. A. Yabuki, Y. Tachibana, I.W. Fathona, Mater. Chem. Phys. **148**, 299 (2014)
41. W. Yang, C. Wang, J. Mater. Chem. C **4**, 7193 (2016)
42. X.S. Li, W.W. Cai, J.H. An, S. Kim, J. Nah, D.X. Yang, R. Piner, A. Velamakanni, I. Jung, E. Tutuc, S.K. Banerjee, L. Colombo, S.R. Ruoff, Science **324**, 1312 (2009)
43. P.W. Sutter, J.I. Flege, E.A. Sutter, Nat. Mater. **7**, 406 (2008)
44. N. Xiao, X. Dong, L. Song, D. Liu, Y. Tay, S. Wu, L.J. Li, Y. Zhao, T. Yu, H. Zhang, W. Huang, H.H. Hng, P.M. Ajayan, Q. Yan, ACS Nano **5**, 2749 (2011)
45. F. Akbar, M. Kolahdouz, S. Larimian, B. Radfar, H.H. Radamsson, J. Mater. Sci. **26**, 4347 (2015)
46. Y. Hernandez, V. Nicolosi, M. Lotya, F.M. Blighe, Z.Y. Sun, S. De, I.T. McGovern, B. Holland, M. Byrne, Y.K. Gun' ko, J.J. Boland, P. Niraj, G. Duesberg, S. Krishnamurthy, R. Goodhue, J. Hutchison, V. Scardaci, A.C. Ferrari, J.N. Coleman, Nat. Nanotechnol. **3**, 563 (2008)
47. X. Huang, Z. Yin, S. Wu, X. Qi, Q. He, Q. Zhang, Q. Yan, F. Boey, H. Zhang, Small **7**, 1876 (2011)
48. X. Huang, X. Qi, F. Boey, H. Zhang, Chem. Soc. Rev. **41**, 666 (2012)
49. L.H. Li, Y.Z. Guo, X.Y. Zhang, Y. Song, J. Mater. Chem. A **2**, 19095 (2014)

50. L.Y. Xu, G.Y. Yang, H.Y. Jing, J. Wei, Y.D. Han, Nanotechnology **25**, 055201 (2014)
51. W. Zhang, E. Bi, M. Li, L. Gao, Colloids Surf A **490**, 232 (2016)
52. J. Liu, L.B. Liu, X.W. Wu, X.K. Zhang, T.D. Li, New J. Chem. **39**, 5272 (2015)
53. W.S. Ma, J.W. Zhou, X.D. Lin, Acta Chim. Sin. **69**, 1463 (2011)
54. M.M. Alam, W. Ji, H.N. Luitel, Y. Ozaki, T. Watari, K. Nakashima, RSC Adv. **4**, 52686 (2014)
55. Y. Wang, Y. Wang, J. Chen, H. Guo, K. Liang, K. Marcus, Q. Peng, J. Zhang, Z. Feng, Electrochim. Acta **218**, 24 (2016)
56. E. Pike, C.H. Seager, Phys. Rev. B **10**, 1421 (1974)
57. L.H. Fang, S. Bin, J.M. Qing, C.P. Wong, Proceeding of 9th International Symposium on Advanced Packaging Materials: Processes, Properties and Interfaces **193** (2014)
58. X. W. Hu, L. H. Li, S. M. Zhao, X. Leng. Adv. Mater. Res. **577**, 287 (2011)